

Cross Sectional Geometry of the Forelimb Skeleton and Flight Mode in Pelecaniform Birds

Erin L. R. Simons,^{1*} Tobin L. Hieronymus,² and Patrick M. O'Connor³

¹Department of Anatomy, Midwestern University, Glendale, Arizona 85308

²Department of Anatomy and Neurobiology, Northeastern Ohio Universities College of Medicine, Ohio

³Department of Biomedical Sciences, Ohio University, Ohio

ABSTRACT Avian wing elements have been shown to experience both dorsoventral bending and torsional loads during flapping flight. However, not all birds use continuous flapping as a primary flight strategy. The pelecaniforms exhibit extraordinary diversity in flight mode, utilizing flapping, flap-gliding, and soaring. Here we (1) characterize the cross-sectional geometry of the three main wing bone (humerus, ulna, carpometacarpus), (2) use elements of beam theory to estimate resistance to loading, and (3) examine patterns of variation in hypothesized loading resistance relative to flight and diving mode in 16 species of pelecaniform birds. Patterns emerge that are common to all species, as well as some characteristics that are flight- and diving-mode specific. In all birds examined, the distal most wing segment (carpometacarpus) is the most elliptical (relatively high I_{\max}/I_{\min}) at mid-shaft, suggesting a shape optimized to resist bending loads in a dorsoventral direction. As primary flight feathers attach at an oblique angle relative to the long axis of the carpometacarpus, they are likely responsible for inducing bending of this element during flight. Moreover, among flight modes examined the flapping group (cormorants) exhibits more elliptical humeri and carpometacarpi than other flight modes, perhaps pertaining to the higher frequency of bending loads in these elements. The soaring birds (pelicans and gannets) exhibit wing elements with near-circular cross-sections and higher polar moments of area than in the flap and flap-gliding birds, suggesting shapes optimized to offer increased resistance to torsional loads. This analysis of cross-sectional geometry has enhanced our interpretation of how the wing elements are being loaded and ultimately how they are being used during normal activities. *J. Morphol.* 272:958–971, 2011. © 2011 Wiley-Liss, Inc.

KEY WORDS: cross-sectional geometry; pelecaniforms; functional morphology; flight behavior

INTRODUCTION

The cross-sectional geometry of long bones has been used as a proxy for estimating resistance to the biomechanical loading encountered by that bone during the life of an organism. More specifically, the shape of the cross-section determines the ability of a given bone to withstand stresses and helps reduce stress and strain under loading

conditions. Parameters derived from beam theory characterize the amount and distribution of cortical bone and have been used to functionally interpret cross-sectional geometry (Roark and Young, 1975). Three commonly used parameters are cortical area (CA), second moment of area (I) and polar moment of area (J). Cortical area represents the amount of cortical bone in a cross-section and has typically been used to estimate resistance to compressional loading. The second moment of area has been used to infer resistance to bending loads, and the polar moment of area has been used to estimate resistance to torsion. Finally, a ratio of two orthogonal second moments provides a measure of relative circularity of the bone shaft. This is functionally relevant as a more elliptical section is typically interpreted to represent a higher resistance to bending in a preferred direction (e.g., Jungers and Minns, 1979; Ruff and Hayes, 1983; Demes et al., 1991; Ruff, 2002; Carlson, 2005).

Cross-sectional geometric approaches have been used extensively to characterize the limb skeleton in terrestrial mammals. However, most birds predominantly occupy the aerial environment where the forelimb skeleton necessarily experiences different types of loads than those encountered by animals on the ground. Generally speaking, it has been argued that the avian postcranial skeleton is optimized for mass reduction (e.g., Bühler, 1992). Moreover, birds are functionally distinct from most

Additional Supporting Information may be found in the online version of this article.

Contract grant sponsors: Ohio University Graduate Student Senate, Ohio University Office of Research and Sponsored Programs (Student Enhancement Award), Ohio University College of Osteopathic Medicine.

*Correspondence to: Erin L. R. Simons, Department of Anatomy, Midwestern University, 19555 N. 59th Ave., Glendale, AZ 85308. E-mail: esimon@midwestern.edu

Received 20 May 2009; Revised 29 December 2010; Accepted 26 February 2011

Published online 12 May 2011 in Wiley Online Library (wileyonlinelibrary.com)
DOI: 10.1002/jmor.10963

nonchiropteran amniotes and it can be assumed that forelimb and hind limb elements are loaded in vastly different ways. In vivo strain-gauge studies of the humerus in both bats and birds indicate that the most proximal limb element is primarily loaded in torsion and dorsoventral bending during flapping flight due to the production of lift forces acting on the wing distal to the humerus (Swartz et al., 1992; Biewener and Dial, 1995). However, not all birds use continuous flapping flight as their primary locomotor mode. As continuous flapping is energetically expensive, many groups of birds have developed novel energy-saving techniques such as various types of gliding and soaring (Norberg, 1985; Rayner, 1988; Rayner et al., 2001). At present it is unclear how different habitual flight modes may affect the loading environment, and thus, the cross sectional geometry, of individual forelimb elements.

The pelecaniforms represent a clade of neognath birds that exhibit an extraordinary diversity in both flight and foraging behaviors (Brewer and Hertel, 2007). Flight characteristics exhibited by birds in this group range from continuous flapping (cormorants and shags) to various types of gliding or flap-gliding (e.g., tropicbirds and boobies) and soaring strategies (e.g., pelicans, gannets). During soaring, birds exploit moving air currents to gain potential energy, making this the least energetically expensive mode of flight (Norberg, 1985). Static soaring birds such as the pelican, frigatebird, and anhinga/darter use rising columns of air, or thermals. By contrast, dynamic soarers such as the gannet utilize velocity differences in stratified currents over the ocean to generate lift. Pelecaniforms forage in a variety of ways: nondiving birds forage either on the wing (frigatebirds) or from the surface (most pelicans); gannets, boobies, and tropicbirds perform spectacular plunge dives; and cormorants and anhingas use foot-propelled pursuit dives to capture prey.

Ongoing research has demonstrated that the external morphology of forelimb bones (humerus, ulna, and carpometacarpus) varies in a predictable way among flight styles, and specifically, that the external mid-shaft diameter of these elements is particularly important for distinguishing among flight modes (Simons, 2010). As such, additional information characterizing the internal morphology of long bones (e.g., cortical thickness and distribution) may be critical for better elucidating specific relationships among whole bone shape, bone cross-sectional properties, whole wing shape and loading regimes associated with different modes of flight in birds.

Several previous studies have investigated long bone cross-sectional geometry in birds across a varied sample of neognaths. Cubo and Casinos (1998) examined the scaling relationship of CA, I in the maximum direction (I_{\max}), and J of the hu-

merus, radius, ulna, as well as hind limb elements. In general, wing bones were found to exhibit isometry under the geometric similarity model (Cubo and Casinos, 1998). In addition, the authors provided data on the orientation of I_{\max} for all elements. For proximal elements (humerus and femur) the maximum I was found to be in the PM-AL (posteromedial-anterolateral) orientation, whereas I_{\max} of the ulna and tibiotarsus was in the PL-AM orientation. More recently, Habib and Ruff (2008) and Habib (2010) examined section moduli (an estimate of structural strength) ratios of the femur and humerus as a way to differentiate among locomotor categories (such as obligate terrestrial runners, perchers, hind limb and forelimb-propelled divers, and dynamic soaring birds; Habib and Ruff, 2008) and to compare the skeletal strength of birds utilizing wing-propelled underwater flight to other avian taxa (Habib, 2010). Although these studies have revealed important patterns of bone shape and/or inferred strength related to locomotor potential and bone loading, neither examined the entire forelimb skeleton in their analysis. Nonetheless, both studies provide important perspectives on avian long bone morphology in general and provide the impetus to further examine cross-sectional geometry of avian wing bones in a phylogenetically restricted, yet flight-mode diverse group such as the pelecaniforms.

The objective of this study is to characterize the cross-sectional geometry of the forelimb elements in pelecaniform birds and to examine the relationship between the cross-sectional geometry and flight mode, and in particular, of those elements to which the primary and secondary flight feathers are attached. We investigate the cortical area (CA), ratio of the maximum to minimum second moments of area (I_{\max}/I_{\min}), and the polar moment of area (J) of the humerus, ulna, and carpometacarpus in the flight and diving mode-diverse pelecaniforms.

MATERIALS AND METHODS

Sixteen species of pelecaniform birds represent the focal sample used in this study (Supporting Information Appendix). Pelecaniforms include Pelecanidae (pelicans), Sulidae (gannets and boobies), Phaethonidae (tropicbirds), Phalacrocoracidae (cormorants and shags), Fregatidae (frigatebirds), and Anhingidae (anhingas and darters). A composite phylogeny (Fig. 1) of taxa used in this analysis was assembled based on the following studies: Siegel-Causey (1988), Friesen and Anderson (1997), Kennedy and Spencer (2004), and Livezey and Zusi (2007). Species were assigned to one of four flight mode categories (flap, flap-glide, static soar, dynamic soar) based on behavioral data collected from the literature (Table 1; e.g., Ashmole, 1971; Pennycuik, 1972; Schnell, 1974; Nelson, 1978; Pennycuik, 1983; Johnsgard, 1993; Hertel and Ballance, 1999; Weimerskirch et al., 2003; also, see Simons, 2010). Species were included within a flight mode category if they habitually utilize that flight behavior. Indeed, all species in this study do flap their wings continuously under specific circumstances, i.e., during

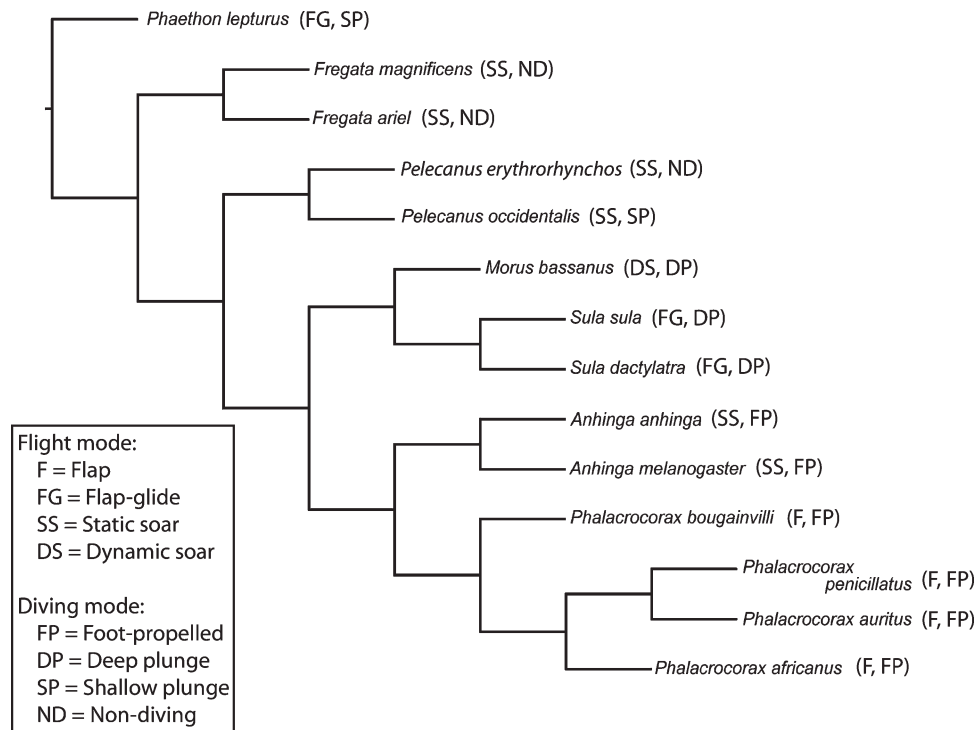


Fig. 1. Composite phylogeny of pelecyaniform taxa used in study, with flight mode and diving mode indicated for each species.

take-off or when wind speeds are not sufficient for soaring (e.g., Owre, 1967; Schnell, 1974; Nelson, 2005). However, in this study we focus on the primary flight mode of each species. Unfortunately, quantified flight behavior data (i.e., flight kinematics and/or time budgets) were unavailable for these species. Observational data was used as a best estimate of primary flight mode.

Adaptation for aquatic locomotion is known to affect cross-sectional properties (Taylor, 1994; Habib and Ruff, 2008; Kriloff et al., 2008; Habib, 2010), and we used two measures to account for the effect of diving mode on cross-section in pelecyaniforms. Species were assigned to one of four diving behavior categories (foot-propelled diving, deep plunge-diving, shallow plunge-diving or nondiving) and maximum recorded dive depth was

included in our analysis as a continuous variable (Table 1; Schreiber et al., 1975; del Hoyo et al., 1992; Hustler, 1992; Johnsgard, 1993; Le Corre, 1997; Garthe, 2000; Ropert-Coudert, 2004; Ryan, 2007; Weimerskirch et al., 2008; Green et al., 2009).

The humerus, ulna, and carpometacarpus (CMC) of 16 species ($n = 94$, mean of 6 specimens per species; Table 1) were scanned on a GE eXplore Locus MicroCT Scanner housed at Ohio University. The mid-shaft region (5–7 cm, encompassing the precise mid-shaft) of each element was scanned once. Although cross-sections have been shown to vary throughout the length of the bone (Ruff and Hayes, 1983), the maximum stress is predicted to occur at mid-shaft (Beer et al., 2006). Wing bones were sampled from the right side of skeletally

TABLE 1. List of taxa scanned with mean species body mass (from Dunning, 2008), flight and diving mode groups, and maximum recorded dive depths

Species	Common name	<i>n</i>	BM (g)	Flight mode	Diving mode	Maximum dive depth (m)
<i>Phalacrocorax auritus</i>	Double-crested Cormorant	10	1,960	Flap	Foot-propelled	7.9
<i>Phalacrocorax africanus</i>	Long-tailed Cormorant	6	545	Flap	Foot-propelled	2.5
<i>Phalacrocorax bougainvillii</i>	Guanay Cormorant	4	2,485	Flap	Foot-propelled	12
<i>Phalacrocorax penicillatus</i>	Brandt's Cormorant	7	2,248	Flap	Foot-propelled	50
<i>Sula dactylatra</i>	Masked Booby	7	1,713	Flap-glide	Deep plunge	6
<i>Sula sula</i>	Red-footed Booby	6	857	Flap-glide	Deep plunge	8
<i>Phaethon lepturus</i>	White-tailed tropicbird	7	334	Flap-glide	Shallow plunge	4
<i>Anhinga melanogaster</i>	Darter	3	1,340	Static soar	Foot-propelled	4
<i>Anhinga anhinga</i>	Anhinga	6	1,235	Static soar	Foot-propelled	4
<i>Fregata ariel</i>	Lesser Frigatebird	7	806	Static soar	Nondiving	N/A
<i>Fregata magnificens</i>	Magnificent Frigatebird	4	1,499	Static soar	Nondiving	N/A
<i>Pelecanus erythrorhynchos</i>	American White Pelican	7	5,650	Static soar	Nondiving	N/A
<i>Pelecanus occidentalis</i>	Brown Pelican	10	3,438	Static soar	Shallow plunge	1
<i>Morus bassanus</i>	Atlantic Gannet	8	3,000	Dynamic soar	Deep plunge	23
<i>Morus capensis</i>	African Gannet	1	2,644	Dynamic soar	Deep plunge	9.7
<i>Morus serrator</i>	Australasian Gannet	1	2,350	Dynamic soar	Deep plunge	23

mature individuals and included both sexes depending on availability of specimens. Within the pelecaniforms, differences in body size between the sexes tend to be small, ranging from 0 to 20% in adults (Johnsgard, 1993). The degree of asymmetry between right and left side wing elements is unknown. Each element was positioned in the μ CT scanner with the long axis of the bone parallel to the scanner bed. A 1 mm diameter circle of barium sulfate was placed at mid-shaft on the three wing elements to ensure a readily identifiable radio-dense marker for use in orienting scan data during subsequent quantitative analyses. A scan resolution of 44–46 μ m was used to acquire cross sections (x-ray tube voltage = 80 kV, x-ray tube current = 450 m). Skeletal specimens were borrowed from the Carnegie Museum of Natural History (CM), National Museum of Natural History (NMNH) and Ohio University Vertebrate Collections (OUVC).

One slice, immediately proximal to the radio-dense marker, from each element was selected for analysis. The following parameters were calculated for each mid-shaft slice using ImageJ version 1.36b (NIH) with MomentMacroJ version 1.3 (www.hopkinsmedicine.org/fae/mmacro.htm): cortical area (CA), total cross-sectional area (TA), second moment of area in the maximum direction (I_{max}), and second moment of area in the minimum direction (I_{min}). The polar moment of area (J) was calculated as the sum of I_{max} and I_{min} . In addition, the total length (L) of each element was measured. Because body mass data were not available for these specific individuals, a geometric mean (GM) was established as a proxy for body size from five additional skeletal measurements: femur length, synsacral length, sternal length, sternal width, and height of sternal keel (Mosimann, 1970; Mosimann and James, 1979; Niemi, 1985; Simons, 2010). Lengths were measured using digital calipers (Mitutoyo Digimatic calipers). All individual measurements were \log_{10} transformed to achieve normal distributions. The following biomechanical variables were calculated for each element: CA/TA, the amount of cortical bone relative to total bone cross-sectional area; I_{max}/I_{min} , a shape ratio indicating resistance to bending; and J/L , length-standardized resistance to torsion. Nonhistorical analysis of variance (ANOVA) with post hoc Tukey-Kramer multiple comparisons was used to examine patterns in cross-sectional geometric parameters common to all pelecaniforms. Only species in which more than one individual was sampled ($n > 1$) were included in the ANOVA. For multivariate analyses, the biomechanical ratios were \log_{10} transformed to remove ratio-induced skew, then range-transformed to a range of (-1, 1) to allow covariance matrix eigenanalysis.

Each variable was tested for phylogenetic signal in Mesquite 2.7.1 (Maddison and Maddison, 2009) by randomly reshuffling the data across the tips of the tree 10,000 times and comparing the results to the measured squared length (number of character steps) in the given tree (Blomberg et al., 2003; Laurin et al., 2004; Kriloff et al., 2008). Significant phylogenetic autocorrelation was present in all variables ($P < 0.0001$) and justified the use of phylogenetic comparative methods (Felsenstein, 1985; Harvey and Pagel, 1991).

Simultaneously testing for relationships between our several cross-sectional and behavioral variables required a multivariate approach. Canonical variates analysis (CVA) is standard technique for examining differences in morphology due to a categorical effect. However, like all standard canonical analyses, CVA does not account for nonindependence due to phylogeny. Although phylogenetically-informed approaches to canonical analyses that use a phylogenetic generalized least-squares (PGLS; Grafen, 1989) framework are available (Revell and Harrison, 2008; Revell, 2009), some of the computational steps of CVA are not readily compatible with PGLS. We have chosen another form of constrained ordination analysis, known as redundancy analysis (RDA; Legendre and Legendre, 1998:579), to examine relationships between cross-sectional variables and behavioral variables in a phylogenetic context. We will refer to our PGLS adaptation of RDA as phylogenetic redundancy analysis (PRDA). All of the subsequent analysis steps were performed in R 2.10.1 (R Development Core Team, 2009) using

components from R packages ape (Paradis et al., 2004) and geiger (Harmon et al., 2008); scripts are available from the authors on request.

Detailed accounts of PGLS and its basis can be found in Grafen (1989), Martins and Hansen (1997), and Garland and Ives (2000). Further material regarding the application of PGLS to canonical analyses can be found in Revell and Harrison (2008) and Revell (2009). The salient point for our analysis is that the phylogenetic generalized least-squares approach accounts for nonindependence due to phylogeny among n taxa by incorporating an $n \times n$ phylogenetic variance-covariance matrix \mathbf{C} . For each taxon i , the diagonal component of the matrix (C_{ii}) contains the total branch length from the root to that taxon. Off-diagonal components (C_{ij}) contain the shared branch length, from the root, of taxa i and j . The phylogenetic generalized least-squares estimate of multiple regression coefficients \mathbf{B} for a regression of an $n \times p$ matrix \mathbf{Y} of species data on an $n \times m$ matrix \mathbf{X} of species data is

$$\mathbf{B} = (\mathbf{X}'\mathbf{C}^{-1}\mathbf{X})^{-1}\mathbf{X}'\mathbf{C}^{-1}\mathbf{Y}, \quad (1)$$

where \mathbf{X}' is the transpose of \mathbf{X} and \mathbf{C}^{-1} is the inverse of \mathbf{C} . If the original data matrices are multiplied by the inverse square root of matrix \mathbf{C} , as

$$\mathbf{T} = \mathbf{C}^{-1/2}\mathbf{X} \quad (2)$$

$$\mathbf{D} = \mathbf{C}^{-1/2}\mathbf{Y}, \quad (3)$$

then the equivalent estimate for \mathbf{B} can be found using the standard least-squares solution on the transformed matrices, as

$$\mathbf{B} = (\mathbf{T}'\mathbf{T})^{-1}\mathbf{T}'\mathbf{D}. \quad (4)$$

Although this is not the exact procedure followed in the analysis, transformation of the original data matrices using the inverse square root of a phylogenetic variance-covariance matrix (PGLS-transform) is the basis of the approach used to account for phylogenetic nonindependence in PRDA, as has been suggested elsewhere for canonical analyses similar to RDA (Rohlf, 2001; Revell and Harrison, 2008).

Although RDA is based on linear regression using continuous variables, it can accommodate categorical variables dummy-coded as orthogonal contrasts (Legendre and Legendre, 1998; Legendre and Anderson, 1999). Each categorical variable with n categories was broken into $n - 1$ continuous variables, one variable each for categories 1 to ($n - 1$). Each category was scored as a positive value for its respective variable, and zero for other variables, with the exception that the n th category was scored as a negative value in all variables as a contrast. Because sample sizes for categories were unequal, values for the positive and contrast score within each variable were adjusted to sum to zero to maintain orthogonality.

The PGLS transformation matrix \mathbf{Z} (equivalent to $\mathbf{C}^{-1/2}$) was calculated by singular value decomposition of \mathbf{C}^{-1} , such that

$$\mathbf{C}^{-1} = \mathbf{\Upsilon}\mathbf{\Lambda}\mathbf{V}', \quad (5)$$

where $\mathbf{\Upsilon}$ and \mathbf{V} are matrices of the left and right singular vectors of \mathbf{C}^{-1} , and $\mathbf{\Lambda}$ is a diagonal matrix of the singular values of \mathbf{C}^{-1} . Matrix \mathbf{Z} was then calculated as

$$\mathbf{Z} = \mathbf{\Upsilon}(\sqrt{\mathbf{\Lambda}})\mathbf{V}'. \quad (6)$$

The complete set of cross-sectional variables ($n \times m$ matrix \mathbf{Y}) and size, maximum dive depth, and dummy-coded orthogonal contrasts for flight and dive behaviors ($n \times p$ matrix \mathbf{X}) were concatenated into a single $n \times (m + p)$ matrix \mathbf{W} . A vector of ancestral character states (a) of length $m + p$ was calculated as

$$a = [(\mathbf{1}'\mathbf{C}^{-1})^{-1}\mathbf{1}'\mathbf{C}^{-1}\mathbf{W}]', \quad (7)$$

where $\mathbf{1}$ is an $n \times 1$ column vector with (1) in each cell. Species data were PGLS transformed and centered on ancestral character states as

$$\mathbf{M} = \mathbf{Z}\mathbf{W} - \mathbf{Z}\mathbf{1}\mathbf{a}' \tag{8}$$

PGLS-transformed data \mathbf{M} were then separated into a matrix of dependent cross-sectional variables \mathbf{D} and a matrix of independent size, flight, and dive-related variables \mathbf{T} . As for the standard computation of RDA, a matrix of multiple regression coefficients, \mathbf{B} , was calculated using equation (4) given previously. A matrix of estimated values of \mathbf{D} based on this regression, $\hat{\mathbf{D}}$, was calculated as

$$\hat{\mathbf{D}} = \mathbf{T}\mathbf{B} \tag{9}$$

Matrix $\hat{\mathbf{D}}$ represents a linear combination of cross-sectional variables and size, dive, and flight-related variables. The central calculation of redundancy analysis is an eigenanalysis of matrix $\hat{\mathbf{D}}$, which results in an ordination of cross-sectional variables that is constrained to include information about size, flight mode, and diving mode. Performing the regression and eigenanalysis on PGLS-transformed data removes the expected effects of shared phylogenetic history on the final ordination space.

Eigenanalysis of $\hat{\mathbf{D}}$ results in a set of eigenvalues Λ and eigenvectors \mathbf{U} . A set of object scores and fitted object scores in PGLS space, \mathbf{P} and $\hat{\mathbf{P}}$ respectively, can be calculated as

$$\mathbf{P} = \mathbf{D}\mathbf{U} \tag{10}$$

$$\hat{\mathbf{P}} = \hat{\mathbf{D}}\mathbf{U} \tag{11}$$

While these scores do not represent an ordination of the data in terms of real (non-PGLS transformed) units, their axis-by-axis correlation provides a measure of the strength of the relationship between morphological and size/behavioral datasets on each ordination axis.

Points in matrix \mathbf{U} provides a direct representation of the ordination space in terms of PGLS-transformed dependent variables \mathbf{D} . To place the PGLS-transformed independent variables \mathbf{T} in the same context, the correlation coefficients of axis-by-axis correlations between \mathbf{T} and $\hat{\mathbf{P}}$ were scaled by $\sqrt{\lambda_i / \sum \Lambda}$, the square root of the proportional variance explained by that axis. Biplots of \mathbf{U} and the scaled correlation coefficients of \mathbf{T} and $\hat{\mathbf{P}}$ provide a direct representation of the relationships between dependent and independent variables in the ordination space after accounting for the effects of phylogeny.

Object scores in species space can be found by substituting the species data from \mathbf{Y} , centered on their phylogenetic means, for \mathbf{D} in equation (10):

$$\mathbf{S} = (\mathbf{Y} - \mathbf{1}\mathbf{a}')\mathbf{U} \tag{12}$$

Scores in \mathbf{S} maintain the morphological relationships between species in Euclidean space, but are not phylogenetically independent. Cluster analysis (UPGMA) of the species scores obtained from PRDA was used to visualize groupings of species utilizing similar flight and diving mode. Ancestral character state analyses of species data and ordination scores were performed in Mesquite 2.71 (Maddison and Maddison, 2009).

RESULTS

Cross-sectional morphology

Results of this study reveal that some common cross-sectional geometric relationships exist among the three forelimb elements in all pelecyaniforms examined (Table 2, Fig. 2). For example in all species the carpometacarpus exhibited a significantly more ($P < 0.0001$) elliptical (higher I_{\max}/I_{\min} ratio) cross section than either the humerus or ulna (Fig. 3A), with the major axis of the carpometacarpus oriented dorsoventrally. Moreover, the humerus exhibited significantly (nonparametric Kruskal-

TABLE 2. Species means of I_{\max}/I_{\min} , length standardized polar moment of area (J/L), and relative cortical area (CA/TA) from raw data for each of the three main forelimb bones in birds (Standard deviation)

Species	Hum	I_{\max}/I_{\min} Uln	Cmc	Hum	J/L Uln	Cmc	Hum	CA/TA Uln	Cmc
<i>Phalacrocorax auritus</i>	1.426 (0.12)	1.110 (0.08)	1.854 (0.15)	1.545 (0.34)	0.545 (0.13)	0.374 (0.06)	0.559 (0.05)	0.609 (0.02)	0.701 (0.02)
<i>Phalacrocorax africanus</i>	1.587 (0.09)	1.165 (0.06)	1.948 (0.13)	0.367 (0.06)	0.135 (0.02)	0.105 (0.02)	0.588 (0.06)	0.611 (0.04)	0.708 (0.05)
<i>Phalacrocorax bougainvillii</i>	1.424 (0.12)	1.133 (0.01)	1.671 (0.18)	1.584 (0.13)	0.561 (0.07)	0.387 (0.04)	0.557 (0.03)	0.566 (0.01)	0.628 (0.03)
<i>Phalacrocorax penicillatus</i>	1.626 (0.07)	1.146 (0.05)	1.711 (0.11)	1.638 (0.26)	0.515 (0.08)	0.337 (0.06)	0.655 (0.03)	0.677 (0.04)	0.759 (0.05)
<i>Sula dactylatra</i>	1.284 (0.10)	1.242 (0.05)	1.533 (0.09)	1.831 (0.29)	0.898 (0.13)	0.857 (0.16)	0.465 (0.03)	0.401 (0.03)	0.425 (0.02)
<i>Sula sula</i>	1.387 (0.08)	1.230 (0.06)	1.497 (0.10)	1.207 (0.11)	0.602 (0.05)	0.483 (0.05)	0.430 (0.02)	0.352 (0.03)	0.414 (0.02)
<i>Phaethon lepturus</i>	1.297 (0.10)	1.361 (0.06)	1.507 (0.11)	0.384 (0.07)	0.190 (0.02)	0.181 (0.03)	0.485 (0.04)	0.518 (0.03)	0.556 (0.02)
<i>Anhinga melanogaster</i>	1.359 (0.08)	1.341 (0.09)	1.409 (0.07)	1.163 (0.19)	0.626 (0.08)	0.416 (0.07)	0.772 (0.05)	0.660 (0.01)	0.753 (0.03)
<i>Anhinga anhinga</i>	1.322 (0.12)	1.520 (0.10)	1.676 (0.18)	1.188 (0.16)	0.755 (0.12)	0.425 (0.10)	0.766 (0.09)	0.687 (0.08)	0.733 (0.08)
<i>Fregata ariel</i>	1.354 (0.07)	1.387 (0.10)	1.653 (0.07)	1.593 (0.13)	0.715 (0.07)	0.695 (0.09)	0.341 (0.02)	0.256 (0.01)	0.299 (0.02)
<i>Fregata magnificens</i>	1.408 (0.10)	1.289 (0.06)	1.584 (0.12)	3.290 (0.44)	1.446 (0.36)	1.329 (0.25)	0.302 (0.02)	0.232 (0.02)	0.292 (0.02)
<i>Pelecanus erythrorhynchos</i>	1.459 (0.13)	1.309 (0.10)	1.514 (0.14)	1.099 (2.10)	3.005 (0.58)	2.678 (0.69)	0.223 (0.02)	0.242 (0.02)	0.302 (0.01)
<i>Pelecanus occidentalis</i>	1.392 (0.09)	1.455 (0.05)	1.473 (0.12)	5.272 (0.76)	1.434 (0.23)	1.434 (0.14)	0.275 (0.04)	0.275 (0.03)	0.284 (0.02)
<i>Morus bassanus</i>	1.188 (0.09)	1.248 (0.04)	1.491 (0.11)	3.128 (0.15)	1.702 (0.16)	1.498 (0.11)	0.503 (0.02)	0.425 (0.03)	0.446 (0.03)
<i>Morus capensis</i>	1.098	1.218	1.442	2.472	1.456	1.175	0.501	0.420	0.496
<i>Morus serrator</i>	1.188	1.241	1.437	2.130	1.187	1.094	0.536	0.455	0.525

Hum: humerus; Uln: ulna, CMC: carpometacarpus.

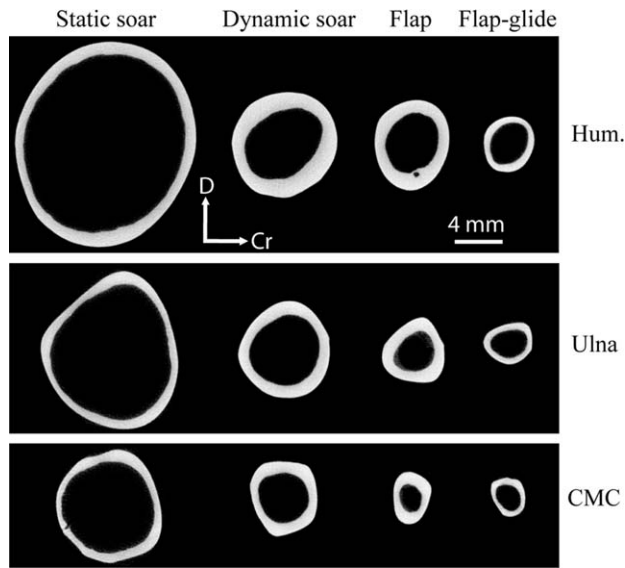


Fig. 2. Example cross-sections of the humerus, ulna, and carpometacarpus (CMC) of four species, representing the four main flight mode categories. Static soarer, *Pelecanus erythrorhynchos* (USNM 13668); Dynamic soarer, *Morus bassanus* (CM S15516); Flapper, *Phalacrocorax auritus* (OUVC 9772); Flap-glide, *Phaethon lepturus* (USNM 490836). Abbreviations: D, indicates dorsal direction; Cr, indicates cranial direction. Scale bar applies to all three rows of cross sections.

Wallis test, $P = 0.0021$) higher J/L than either the ulna or carpometacarpus (Fig. 3B). Relative cortical area (CA/TA) did not differ significantly ($P = 0.6157$) among the three elements (Fig. 3C).

PRDA results

The first three ordination axes from PRDA explain over 98% of the variance present in the PGLS-transformed data (Table 3). All three of these axes show significant correlations between PGLS-transformed object scores \mathbf{P} and PGLS-transformed fitted object scores $\hat{\mathbf{P}}$ (Table 4). Distance biplot scores (Table 5, Figs. 4A,B and 5A,B) show effects of size and flight on the first and third axes, and diving on the second axis.

Notable differences were detected in cross-sectional geometry among the flight mode groups. The flapping group exhibited more elliptical (higher I_{\max}/I_{\min} ratio) carpometacarpi and humeri, and less elliptical ulnae, than other flight modes, placing them on the upper end of the third canonical axis (Fig. 4B).

For all three elements the soaring birds (dynamic + static) generally exhibited higher relative polar moments (J/L) than the flap and flap-gliding birds, and thus occupied the upper end of the first canonical axis (Fig. 4A). Relative polar moment also shows a positive allometric relationship with body size. A UPGMA cluster analysis using the Euclidean distances between species

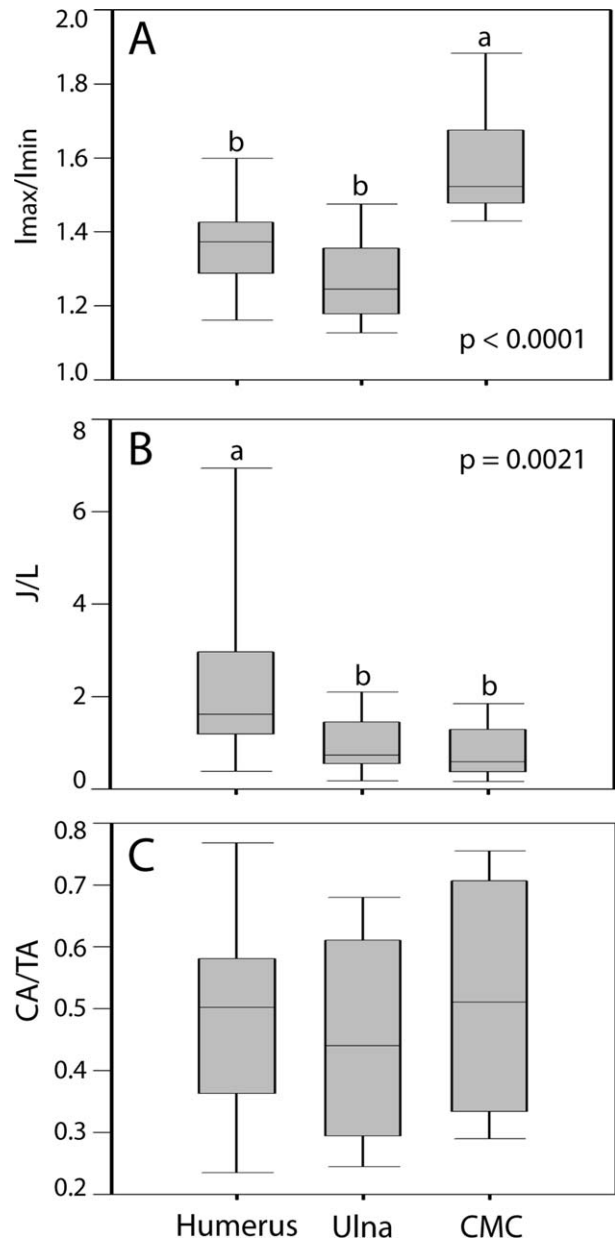


Fig. 3. ANOVA results for pooled species means for the humerus, ulna, and carpometacarpus (CMC): (A) I_{\max}/I_{\min} , (B) Length standardized polar moment of area (J/L), (C) Relative cortical bone area (CA/TA). Significant differences indicated by lowercase letters: a, b. Median line shown in boxes. Whiskers represent 10th and 90th percentiles.

scores on the first and third canonical axes recovers some of the original flight mode categories with an overprinted signal of body size (Fig. 6A).

TABLE 3. Variance explained by PRDA axes

	1st axis	2nd axis	3rd axis	4th axis
Proportion of variance	0.8333	0.0877	0.0599	0.0107
Cumulative proportion of variance	0.8333 ^a	0.921	0.9809	0.9916

^aSignificance under a broken stick model.

TABLE 4. Correlations between ordination vectors in ordination space *D* (species scores) and ordination space *T* (fitted species scores)

	<i>r</i>	<i>P</i>	95% CI for <i>r</i>
1st axis	0.95	<0.0001 ^{a,b}	0.85–0.98
2 nd axis	0.9	<0.0001 ^{a,c}	0.73–0.97
3 rd axis	0.77	0.0005 ^{a,c}	0.44–0.91
4 th axis	0.83	<0.0001 ^a	0.57–0.94

These correlations represent the strength of association between the morphological data in **D** and the size/behavioral model of morphology in **D**, and should be interpreted together with the cumulative proportions of variance given in Table 3.

^aSignificant correlation.

^bSignificant proportion of variance by broken stick.

^cSignificant proportion of variance up to 95% cumulative proportional variance.

Differences in relative cortical area (CA/TA) corresponded to differences in diving behavior (Fig. 5A, B), with a marked positive correlation between relative cortical area and maximum dive depth along the second canonical axis. Nondiving birds were scored as a contrast variable for other diving behavior modes, and thus cannot be represented on the independent variable biplot, but exemplars (e.g., *Fregata magnificens*) cluster at low values of the second canonical axis. A UPGMA cluster analysis using Euclidean distances between species scores on the second canonical axis recovers the original diving behavior categories, with the exception of shallow plunge-diving (Fig. 6B).

DISCUSSION

Patterns common to all pelecaniforms

A more elliptical bone cross-section is interpreted to represent higher resistance to bending in a preferred direction. Of the three elements examined, the CMC is the most elliptical at mid-shaft in roughly the dorsoventral direction (Fig. 3). This suggests that for all flight modes, the CMC may be experiencing primarily bending loads. This may pertain to the way in which feathers transmit aerodynamic forces to the bone. The primary flight feathers (i.e., those attached to the dorsal margin of the CMC) are attached obliquely to the long axis of the CMC (Fig. 7). Moreover, primary flight feathers that attach to the phalanges of the major digit are oriented even more obliquely to the long axis of these elements, and these in turn would induce a bending load on the distal end of the carpometacarpus. This contrasts markedly with the nearly perpendicular manner in which secondary flight feathers attach to the ulna during the downstroke (and when the aerodynamic-induced loads on the bone would be maximal). We suggest that when lift is generated on the primary flight feathers, this orientation of feather attachment to the CMC (and major digit phalanges) would impart

bending loads through a roughly dorsoventral plane (around the craniocaudal axis). Note: we restricted our analysis to the major metacarpal (i.e., the main component of the CMC and the attachment site of the primary flight feathers) and did not characterize the cross section of the minor metacarpal (Fig. 7). It is clear that the compound nature of the element would provide additional support and reduces the amount of bending possible along a craniocaudal plane (around the dorsoventral axis). Thus, the bone may be more likely to bend through a dorsoventral plane and structural (shape) adaptation of the major metacarpal reflects a response over evolutionary time. Indeed, an ancestral state reconstruction analysis using parsimony of the shape ratio of the CMC indicates a general increase in ellipticality of the cross-section of the CMC (Fig. 8).

Within limb analyses of J/L reveal relatively high resistance to torsional loads (increased J/L) in the humeri of all pelecaniforms (Fig. 3). This is consistent with the concept that torsional loads applied to distal elements are additive from distal to proximal through the wing. In addition, this interpretation is supported by the concept that lift generated by the airfoil (secondary flight feathers or wing membrane), distal to the humeral axis, transmits torsional loads to the humerus, as indicated by in vivo strain gauge analyses (Swartz et al., 1992; Biewener and Dial, 1995). It is important to note that the interpretation of J as a measure of resistance to torsion is most robust when the shape ratio of the section (I_{\max}/I_{\min}) is less than or equal to 1.5 (i.e., it is relatively circular;

TABLE 5. Distance biplot scores for PGLS transformed dependent (morphology, **D**) and independent (body size and behavior, **T**) variables, by PRDA axis

Variable	1st axis	2nd axis	3rd axis
Dependent variables			
Humeral J/L	0.6640*	-0.1491	0.1967
Humeral CA/TA	-0.0936	-0.4832*	-0.1351
Humeral I_{\max}/I_{\min}	-0.2902	-0.0505	0.5426*
Ulnar J/L	0.4639	0.066	-0.1836
Ulnar CA/TA	-0.092	-0.5327*	-0.1545
Ulnar I_{\max}/I_{\min}	-0.2222	0.4465	-0.6133*
Carpometacarpal J/L	0.4056	0.0005	-0.1828
Carpometacarpal CA/TA	-0.1235	-0.5032*	-0.3751
Carpometacarpal I_{\max}/I_{\min}	-0.1154	0.032	0.2018
Independent variables			
logGm	0.8959	-0.0174	0.0272
Flapping flight	-0.1917	0.0195	0.1195
Flap-gliding flight	-0.2989	-0.0317	0.0223
Dynamic soaring	0.0696	0.0592	0.0058
Max dive depth	0.0878	0.1714	0.086
Foot-propelled diving	-0.2887	0.14	-0.0395
Deep plunge-diving	-0.2151	0.0606	-0.0655
Shallow plunge-diving	-0.3027	0.0451	-0.0726

Bolded biplot scores indicate major dependent and independent contributors to each axis.

*Eigenvector values for dependent variables greater than the equilibrium contribution length (0.4714).

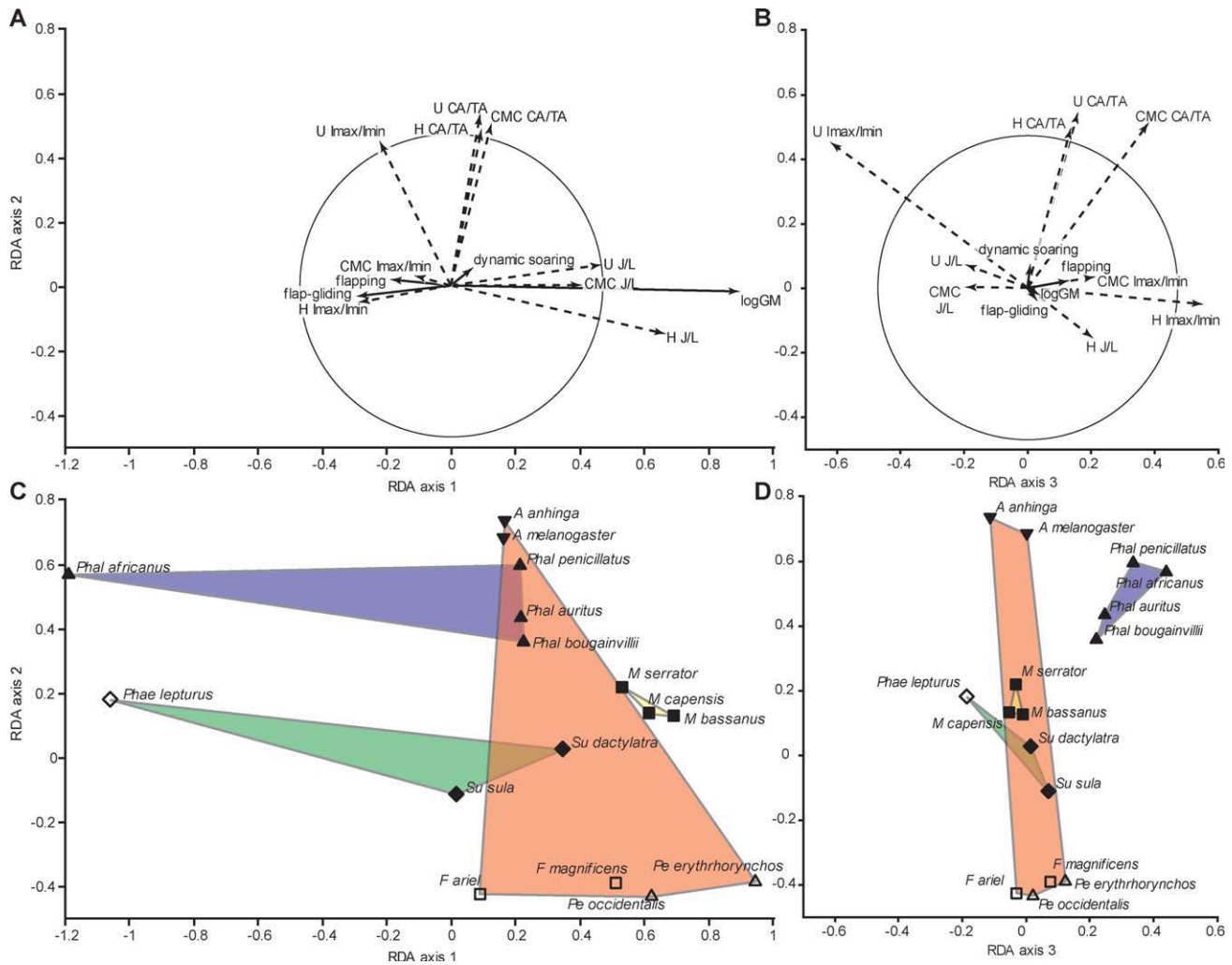


Fig. 4. PRDA ordination of cross-sectional morphology on combined body size, flight behavior, and diving behavior data. **NOTE:** Both flight and diving variables are considered simultaneously in this ordination, but each class of effect will be shown separately for clarity. (A, B) Biplots of the effects of cross-sectional variables D (dashed lines) with body size (logGM) and flight variables (solid lines) on PRDA axes 1 and 2 (A) and PRDA axes 3 and 2 (B). Correlation between two variables is approximated by the angle between their respective rays—acute angles indicate positive correlation, obtuse angles indicate negative correlation, and right angles indicate the absence of correlation. The circle represents the expected equilibrium contribution of cross-sectional variables to the ordination axes. Dashed lines projecting beyond this circle represent cross-sectional variables that make significant contributions to their respective axes; in this case inferred resistance to torsional loads for the humerus on axis 1, relative humeral, ulnar, and carpometacarpal cortical area on axis 2, and humeral and ulnar bending resistance on axis 3. Note that body size, as approximated by logGM, loads heavily on the first axis, and is negatively correlated with both flapping and flap-gliding modes of flight. In contrast, flapping flight is the independent variable with greatest effect on axis 3, and is positively correlated with carpometacarpal and humeral bending resistance. (C, D) Species scores \mathbf{Y} plotted onto the ordination spaces defined in (A) and (B), with convex hulls around categories of flight mode. Color key for flight mode: Purple = Flap, Green = Flap-glide, Orange = Static soar, Yellow = Dynamic soar. Note that both forms of soaring are loosely associated with larger body sizes on axis 1, while flapping flight stands out from other flight modes on axis 3. Species points on this plot are not PGLS transformed, and they represent the actual Euclidean distances of species data in the ordination space, including phylogenetic signal. Biplot rays show the effect of PGLS-transformed variables D on the ordination axes, which reflects correlations between variables while taking phylogeny into account. This difference causes some misalignment between PGLS-transformed independent variables (e.g., flapping on axis 1) and their non-PGLS transformed exemplars (e.g., the position of phalacrocoracids on axis 1).

Daegling, 2002). The mean I_{\max}/I_{\min} of the humerus and ulna for all flight modes, with the exception of the humerus of the flapping group, is less than 1.5.

The proportion of cortical bone per total bone area (CA/TA) is not significantly different among the three elements for pelecaniform taxa (Fig. 3C). Whereas there are differences among taxa (and

indeed among flight modes, see below), within each species CA/TA is consistent for the three elements. For example, *Pelecanus occidentalis* exhibits the lowest values for CA/TA, ranging from 0.22 for the humerus to 0.28 for the CMC (Table 2). This differs greatly from *Anhinga melanogaster*, which exhibits CA/TA values of 0.66–0.77. Within each of these species, however, the results for the

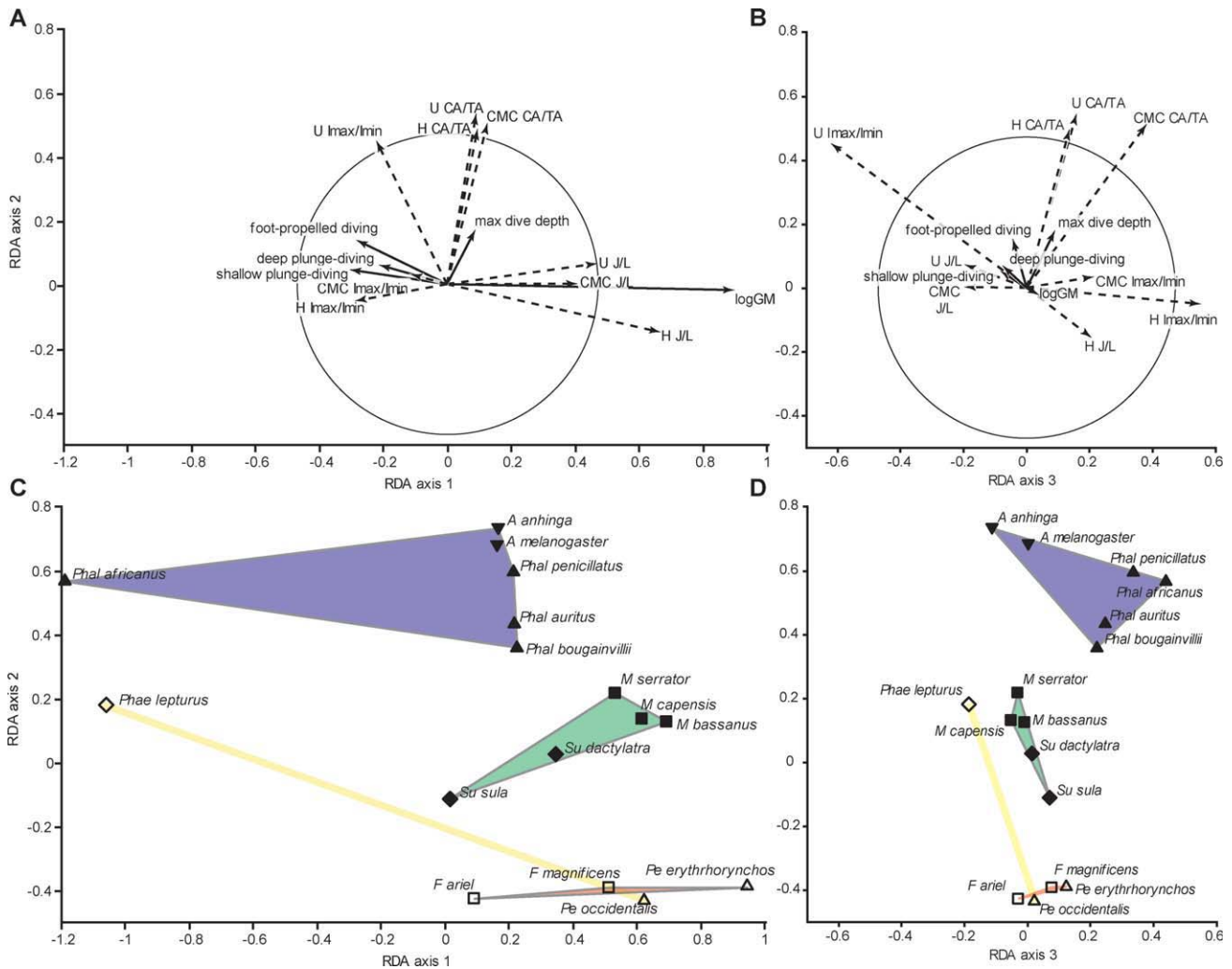


Fig. 5. PRDA ordination of cross-sectional morphology on combined body size, flight behavior, and diving behavior data. (A, B) Biplots of the effects of cross-sectional variables D (dashed lines) with body size (logGM) and diving behavior variables (solid lines) on PRDA axes 1 and 2 (A) and PRDA axes 3 and 2 (B). Representation of variables as in Figure 4. Note the marked positive correlation between relative cortical area and maximum dive depth on axis 2. (C, D) Species scores plotted onto the ordination spaces defined in (A) and (B), with convex hulls around categories of diving behavior. Color key for flight mode: Blue = Foot-propelled, Green = Deep plunge, Orange = Nondiving, Yellow = Shallow plunge. Note the separation of diving behaviors on axis 2, with foot-propelled diving and deep plunge-diving taxa showing generally positive scores, and nondiving taxa showing negative scores.

three elements are similar. Such differences likely pertain to skeletal variation in the locomotor apparatus between these two species, and specifically, variation that marks buoyancy requirements for different types of foraging behavior (see below). This suggests that for cortical area, the bones of the entire wing (and perhaps the entire skeleton; see O'Connor, 2009) are responding to similar pressures, whether environmental, behavioral, or phylogenetic.

Flight mode patterns

There are also clear differences in cross-sectional characteristics when examined as a function of flight and diving mode categories. The flapping

flight group is separated from other flight mode groups on the 3rd axis of the PRDA based on possessing a more elliptical humerus and CMC (Fig. 4B, D). This suggests that carpometacarpi and humeri of continuously-flapping birds may be experiencing predominantly bending loads, at least more so than the corresponding bones of birds that utilize other (i.e., noncontinuous flapping) primary flight modes such as soaring. Specifically, the CMC exhibits a dorsoventrally elliptical cross section, a shape that is consistent with resistance to bending loads from the obliquely oriented primary flight feathers (Fig. 7). In addition, the relatively elliptical humerus (also with a major axis oriented dorsoventrally) in the flapping flight category suggests that during continuous flapping, even the

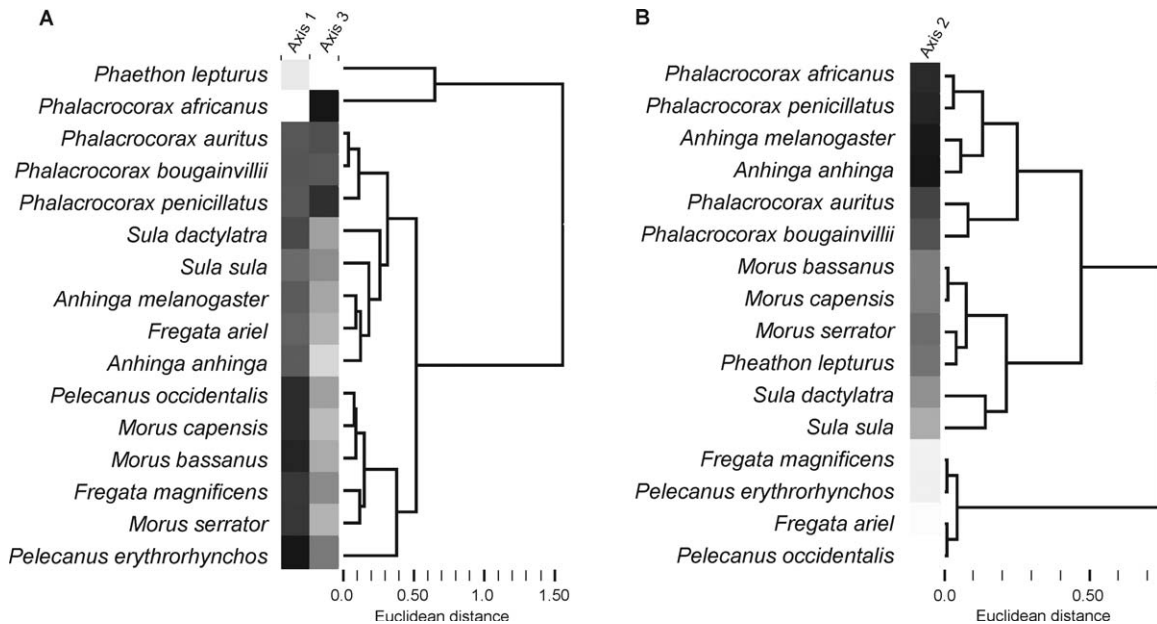


Fig. 6. UPGMA cluster analyses of species scores on the first and third (A) and second (B) canonical axes. (A) Clusters of note on the first and third axes include a group of large-size dynamic and static soarers (*Morus*, *Pelecanus*), a group of medium-size static soarers (*Anhinga*) that group closely with medium-size flap-gliders (*Sula*), a group of obligate flappers (*Phalacrocorax*), and the two smallest taxa in the analysis. (B) Clusters of note on the second axis include the foot-propelled divers (*Anhinga*, *Phalacrocorax*), most of the plunge divers (*Sula*, *Morus*, *Phaethon*), and nondiving pelecaniforms plus *P. occidentalis*.

proximal-most element may be experiencing predominantly bending loads. This may pertain to the frequency of loading experienced by the elements of the continuous-flapping category. For example, the flapping birds examined in this study (cormorants, shags) exhibit wing beat frequencies exceeding five beats per second (Meinertzhagen, 1955; Pennycuick, 1983; Pennycuick, 1990). By contrast, the nonflapping specialists, such as the pelican, exhibit average wing beat frequencies of approximately two beats per second (Johnsgard, 1993). Thus, flapping flight would necessarily result in a higher frequency of wing loading in birds. Recall, all species included in this study are capable of flapping to some degree during take-off or when wind speeds for soaring decrease. Presumably the skeletal elements of all species are built to withstand this occasional flapping. However, the species included in the continuous flapping primary flight mode group experience near-constant, higher frequency flapping than those in the other flight mode groups, and in turn, appear to exhibit bone distributions optimized to resist such loading conditions. Taken together, the relatively high wing-beat frequency of flapping flight, combined with the inferred orientation of the applied load, is here hypothesized to influence structural adaptation of the avian wing skeleton. This interpretation is consistent with the results of Biewener and Dial (1995), who used in vivo strain gauges on the pigeon humerus and documented both dorsoventral bending and torsion during high frequency

flapping flight. In sum, it is clear that additional experimental work is required to examine potential loading differences in birds utilizing different flight modes. Importantly, the cross-sectional geometric differences identified herein will allow the development of specific hypotheses that take into account both shape and flight mode variation.

The carpometacarpus has also received recent focus in the context of a whole-bone metric analysis of the wing skeleton in pelecaniforms. Simons (2010) documented that total length and dorsoventral diameter of the CMC was useful for distinguishing among most flight modes. Interestingly, the flappers in the whole-bone study (cormorants, shags) were not completely separated from all other flight mode groups based on these specific external measures, and instead, overlapped in morphospace with the static soaring pelicans. By incorporating the internal structure of the bones, as in the calculation of I_{\max}/I_{\min} here, increased resolution is gained for exploring the flapping/static soaring interface. Whereas the two groups have similar relative dorsoventral CMC external diameter (relative to total wing size), the cross-sectional shape is different and thereby useful for more fine-tuned separation of the flight modes.

The mainly nondiving static and dynamic soaring birds occupy the upper end of the first canonical axis, which is represented by large body size and large relative polar moments (Fig. 4A, C). The polar moment of the humerus is the only polar moment variable to make a significant contribution

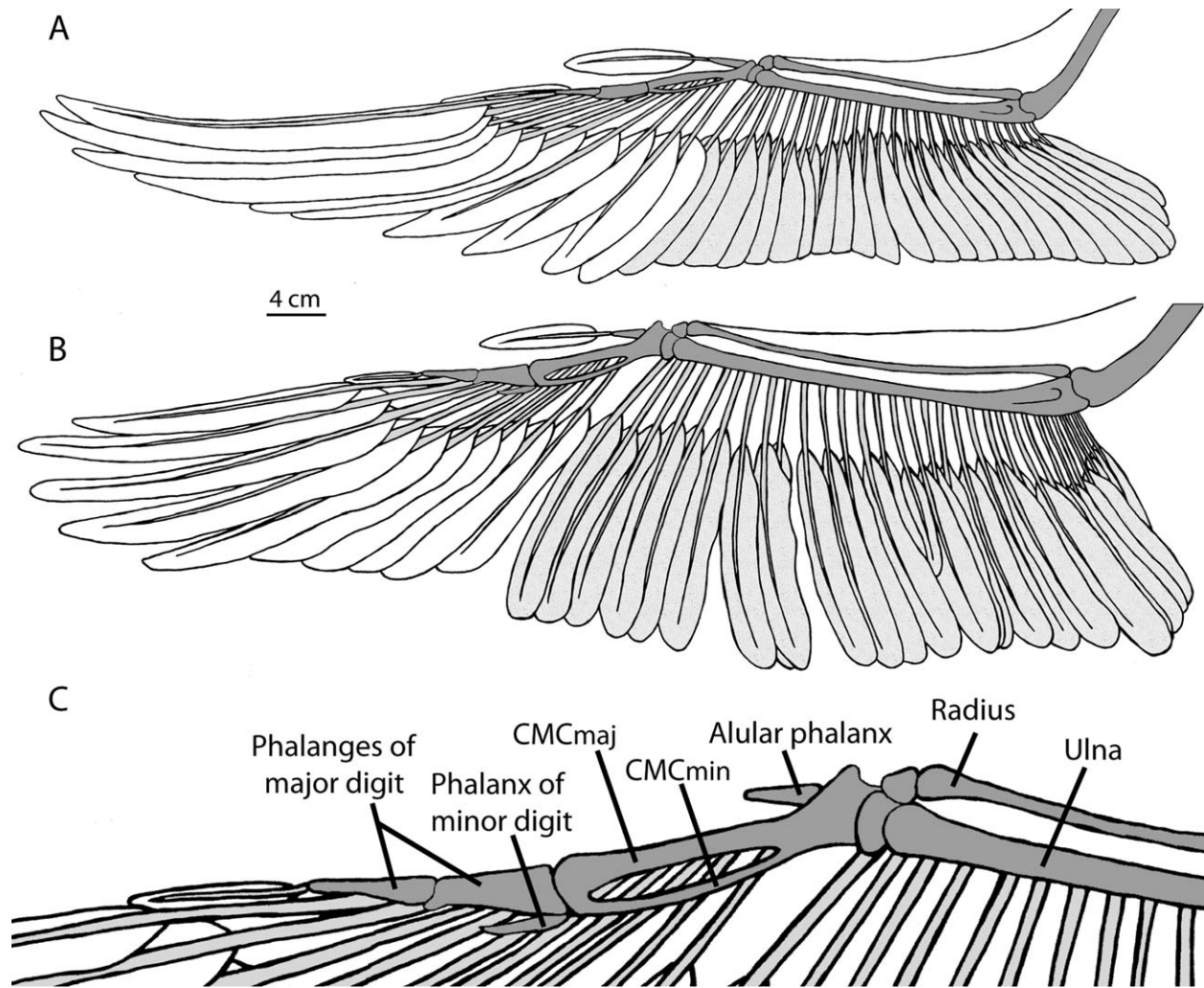


Fig. 7. Illustration of wing anatomy of (A) *Morus bassanus* (OUVC 10587) and (B) *Pelecanus occidentalis* (OUVC 10586) in ventral view. (C) Schematic of the distal forelimb skeleton and proximal feather attachments. The secondary flight feathers (shaded light gray in A and B) are oriented perpendicular to the axis of the ulna. The primary flight feathers are oriented obliquely to the axis of the carpometacarpus. Note also difference in mean chord length (width of wing) between species. Abbreviations: CMCmaj, major metacarpal; CMCmin, minor metacarpal.

to the PRDA axes and relative humeral polar moment exhibits positive allometry, meaning that large size birds exhibit relative polar moments that are larger than expected for their body size. As expected, the largest bird in the study, the American white pelican (mean body mass of 5,650 g, Dunning, 2008) is positioned furthest to the right along PRDA axis 1. However, in addition, the magnificent frigatebird (mean body mass of 1,499 g, Dunning, 2008) is smaller in size than most birds in the Flap group, but is also positioned to the far right along axis 1. This static soaring frigatebird exhibits a relative humeral polar moment more than double in value than that of the flapping cormorants (Table 2). Relatively large polar moment values suggest that a bone is shaped to resist one of several loading environments: bending moments that are not large or frequent enough to require an

elliptical section, predominant/frequent bending that is occurring, but in multiple directions (Carlson, 2005), or that torsion is the predominant load encountered. As element cross-sections in soaring birds clearly exhibit a circular section with material distributed distant from the neutral axis (Fig. 2), we suggest that soaring is indeed placing higher torsional loads on the wing skeleton, and in particular, the humerus. Characteristics that support this interpretation include the fact that soaring birds typically have very large, broad wings. Soaring birds exhibit wings with a relatively high aspect ratio, and in static soaring birds in particular, a significantly longer chord length (Fig. 7). Such long secondary feathers would act as longer lever arms on the ulna as lift is generated, ultimately transferring relatively larger torsional loads up through the humerus. Experimental stud-

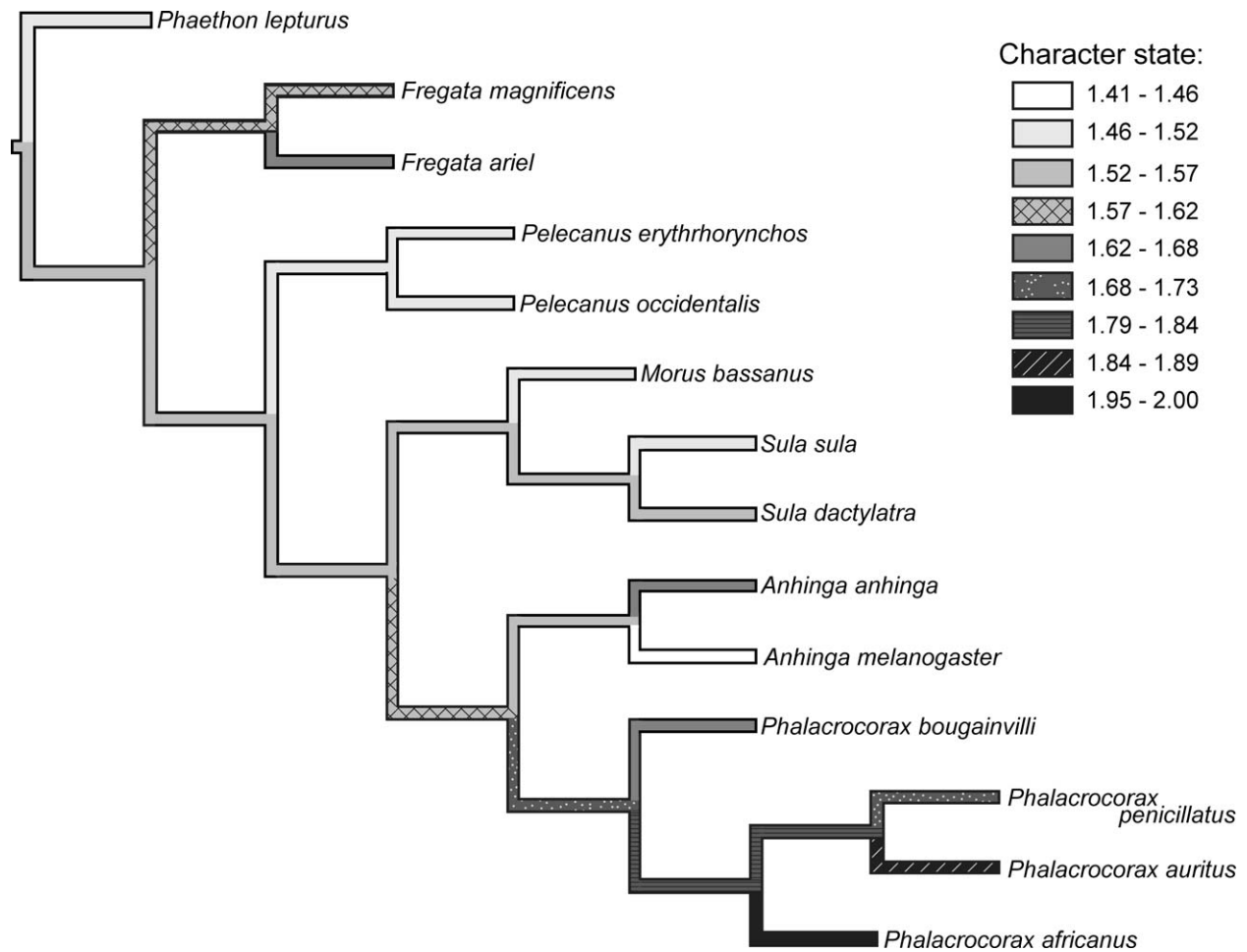


Fig. 8. Ancestral character reconstruction values (using Parsimony) of the shape ratio (I_{\max}/I_{\min}) of the carpometacarpus are mapped on the phylogeny of pelecaniform species. Character state bins are indicated in the key. Not all character state bins are represented on the phylogeny.

ies have shown that, in general, avian humeri experience torsional loads (Biewener and Dial, 1995), but this is one of the first studies to postulate how the shape of the whole wing (including feathers) may differentially impact the amount of torsional loading experienced by the forelimb skeleton (see also de Margerie et al., 2005). As predicted, the birds in this study with large broad wings (pelicans) do indeed have skeletal elements that exhibit higher resistance to torsional loads than birds with smaller, more slender wings. Interestingly, the dynamic soaring bird in the sample (the gannet) possesses a high aspect ratio, but relatively slender wings (shorter chord length). The gannet also exhibits forelimb elements with cross sections optimized to resistant to torsion, suggesting that the wing shape and soaring behavior both affect the loading environment acting on the wings.

Cortical bone area is generally considered in association with resistance to compression in terrestrial animals. Whereas the forelimb bones of

most birds are likely not experiencing significant and/or sustained axial compression, major differences in relative cortical area were identified among different diving mode categories, namely along PRDA axis 2 (Fig. 5). The foot-propelled pursuit divers are separated from all other dive mode categories and exhibit high relative cortical areas in all three elements. Most notably, darters and anhingas (*Anhinga*) exhibit extremely high CA/TA values. Anhingas and darters are highly specialized for sustained underwater foraging. Unlike any other bird examined, anhingas and darters rarely swim at the surface of the water and instead often swim submerged with only their head and neck above the surface. In addition, during foraging they remain totally submerged for up to a minute to stealthily stalk their prey (Owre, 1967; Johnsgard, 1993; Nelson, 2005). Relatively thicker cortical walls may work to impart a reduction in whole-body buoyancy that would be beneficial in this type of foraging strategy. It is also

notable in that *Anhinga* is the only member of peleciforms with a completely pneumatic postcranial skeleton, whereas other members of the clade variably exhibit air-filled bones (O'Connor, 2009). *Phalacrocorax* (cormorants), also exhibit relatively high CA/TA values and a general reduction in whole-body skeletal pneumaticity (although not to the extreme level of pneumaticity observed in *Anhinga*). The deep plunge divers (gannets and boobies) and one shallow plunge diver (tropicbird) are located in the middle of axis 2, clearly separated from both the foot-propelled divers and the nondivers. Clustering tightly with the nondivers is the other shallow plunge diver, the brown pelican. The brown pelican is the only pelican that performs shallow plunge dives, and indeed is so buoyant that it barely becomes submerged during a dive (Schreiber et al., 1975). Thus, in peleciforms, a relatively thick cortical wall may not reflect increased resistance to axial loading, but more likely represents a skeletal modification related to buoyancy reduction in underwater foragers. Similar adaptations have been suggested in other diving specialists among both birds (e.g., auks and penguins) and mammals (Taylor, 1994; Habib and Ruff, 2008; Kriloff et al., 2008; Habib, 2010).

In conclusion, some general patterns emerge when considering the cross-sectional geometry of the wing skeleton in peleciform birds. Importantly, some trends appear independent of flight and diving mode, whereas others partition along these behavioral categories. For all peleciforms, the carpometacarpus is the most elliptical of all limb elements, likely reflecting the manner in which primary flight feathers attach to the long axis of the bone and transmit aerodynamic loads to the skeleton. In contrast, the humerus exhibits the highest polar moment of area (a metric of resistance to torsional loading) of the three limb segments. This is interpreted to reflect a response to the generation of lift distal to the humeral axis during any flight style and the additive nature of torsional loads from proximal to distal through the wing. High relative cortical area was identified in foot-propelled divers such as *Anhinga* and *Phalacrocorax*, suggesting a role in buoyancy modulation. Among flight modes, flapping birds exhibit the most elliptically-shaped bones, whereas soaring birds, especially static soarers, exhibit circular cross sections with bone distributed relatively distant from the hypothesized neutral axis. This analysis of long-bone cross-sectional anatomy has enhanced our interpretation of how avian wing elements relate to hypothesized loading regimes, and generally, how the postcranial skeleton reflects locomotor and foraging activities in birds. Future in vivo studies, especially of distal wing elements, are necessary to test and further refine the hypotheses developed herein related to wing-bone

cross sectional shape, whole-wing morphology and flight mode variation in birds.

ACKNOWLEDGMENTS

The authors thank S. Rogers and B. Livezey (Carnegie Museum of Natural History) and J. Dean and S. Olson (National Museum of Natural History) the curators and collection managers for access to specimens in their collections. They also thank L. Witmer and R. Ridgely for assistance at the Ohio University microCT facility, and S. Williams, B. Patel, C. Ruff, M. Habib, L.N. Cooper, and C. Vinyard for their invaluable discussion.

LITERATURE CITED

- Ashmole NP. 1971. Sea bird ecology and the marine environment. In: Farner DS, King JR, editors. *Avian Biology*, Vol. 1. New York and London: Academic Press. pp 223–286.
- Beer FB, Johnston ER, DeWolf JT. 2006. *Mechanics of Materials*. New York: McGraw.
- Biewener AA, Dial KP. 1995. In vivo strain in the humerus of pigeons (*Columba livia*) during flight. *J Morphol* 225:61–75.
- Blomberg SP, Garland T Jr, Ives AR. 2003. Testing for phylogenetic signal in comparative data: Behavioral traits are more labile. *Evolution* 57:717–745.
- Brewer ML, Hertel F. 2007. Wing morphology and flight behavior of peleciform seabirds. *J Morphol* 268:866–877.
- Bühler P. 1992. Light bones in birds. In: Campbell KEJ, editor. *Papers in Avian Paleontology Honoring Pierce Brodkorb*. Los Angeles: Natural History Museum of Los Angeles County. pp 385–393.
- Carlson KJ. 2005. Investigating the form-function interface in African apes: Relationships between principal moments of area and positional behaviors in femoral and humeral diaphyses. *Am J Phys Anthropol* 127:312–334.
- Cubo J, Casinos A. 1998. Biomechanical significance of cross-sectional geometry of avian long bones. *Eur J Morphol* 36:19–28.
- Daegling DJ. 2002. Estimation of torsional rigidity in primate long bones. *J Hum Evol* 43:229–239.
- Demes B, Jungers WL, Selpien K. 1991. Body size, locomotion, and long bone cross-sectional geometry in indriid primates. *Am J Phys Anthropol* 86:537–547.
- Dunning JB Jr. 2008. *CRC Handbook of Avian Body Masses*. CRC Press, Taylor & Francis Group, Boca Raton, FL.
- Felsenstein J. 1985. Phylogenies and the comparative method. *Am Naturalist* 125:1–12.
- Friesen VL, Anderson DJ. 1997. Phylogeny and evolution of the Sulidae (Aves: Pelecaniformes): A test of alternative modes of speciation. *Molecular Phylogenetics & Evolution* 7:252–260.
- Garland T Jr, Ives AR. 2000. Using the past to predict the present: Confidence intervals for regression equations in phylogenetic comparative methods. *Am Naturalist* 155:346–364.
- Garthe S, Benvenuti S, Montevecchi WA. 2000. Pursuit plunging by northern gannets (*Sula bassana*) feeding on capelin (*Mallotus villosus*). *Proc R Soc B* 267:1717–1722.
- Grafen A. 1989. The phylogenetic regression. *Phil Trans R Soc B* 326:119–157.
- Green JA, White CR, Bunce A, Frappell PB, Butler PJ. 2009. Energetic consequences of plunge diving in gannets. *Endang Species Res* 10:269–279.
- Habib MB, Ruff CB. 2008. The effects of locomotion of the structural characteristics of avian long bones. *Zool J Linn Soc* 153:601–624.
- Habib M. 2010. The structural mechanics and evolution of aquaflying birds. *Biol J Linn Soc* 99:687–698.

- Harvey PH, Pagel MD. 1991. *The Comparative Method in Evolutionary Biology*. Oxford: Oxford University Press.
- Hertel F, Ballance LT. 1999. Wing ecomorphology of seabirds from Johnston Atoll. *Condor* 101:549–556.
- Harmon LJ, Weir JT, Brock CD, Glor RE, Challenger W. 2008. GEIGER: Investigating evolutionary radiations. *Bioinformatics* 24:129–131.
- del Hoyo J, Elliot A, Sargatal J, editors. 1992. *Handbook of the Birds of the World, Vol. 1. Ostrich to Ducks*. Lynx Edicions. Barcelona.
- Hustler K. 1992. Buoyancy and its constraints on the underwater foraging behavior of Reed Cormorants *Phalacrocorax africanus* and Darters *Anhinga melanogaster*. *Ibis* 134:229–236.
- Johnsgard PA. *Cormorants, Darters, and Pelicans of the World*. Washington: Smithsonian Institution Press. 445 p.
- Jungers WL, Minns RJ. 1979. Computed tomography and biomechanical analysis of fossil long bones. *Am J Phys Anthropol* 50:285–290.
- Kennedy M, Spencer HG. 2004. Phylogenies of the Frigatebirds (Fregatidae) and Tropicbirds (Phaethonidae), two divergent groups of the traditional order Pelecaniformes, inferred from mitochondrial DNA sequences. *Mol Phylogenet Evol* 31:31–38.
- Kriloff A, Germain D, Canoville A, Vincent P, Sache M, Laurin M. 2008. Evolution of bone microanatomy of the tetrapod tibia and its use in palaeobiological inference. *J Evol Biol* 21:807–826.
- Laurin M, Girondot M, Loth M-M. 2004. The evolution of long bone microanatomy and lifestyle in lissamphibians. *Paleobiology* 30:589–613.
- Le Corre M. 1997. Diving depths of two tropical Pelecaniformes: The Red-tailed tropicbird and the Red-footed booby. *Condor* 99:1004–1007.
- Legendre P, Anderson MJ. 1999. Distance-based redundancy analysis: Testing multispecies responses in multifactorial ecological experiments. *Ecol Monographs* 69:1–24.
- Legendre P, Legendre L. 1998. *Numerical Ecology*. Amsterdam: Elsevier Science BV. 853 p.
- Livezey BC, Zusi RL. 2001. Higher-order phylogenetics of modern Aves based on comparative anatomy. *Neth J Zool* 51:179–205.
- Maddison WP, Maddison DR. 2009. *Mesquite: A modular system for evolutionary analysis*. Version 2.71. Available at <http://mesquiteproject.org>.
- de Margerie E, Sanchez S, Cubo J, Catanet J. 2005. Torsional resistance as a principal component of the structural design of long bones: Comparative multivariate evidence in birds. *Anat Rec* 282A:49–66.
- Martins EP, Hansen TF. 1997. Phylogenies and the comparative method: A general approach to incorporating phylogenetic information into the analysis of interspecific data. *Am Nat* 149:646–667.
- Meinertzhagen R. 1955. The speed and altitude of bird flight. *Ibis* 97:81–117.
- Mosimann JE. 1970. Size allometry: Size and shape variables with characterizations of the lognormal and generalized gamma distributions. *J Am Stat Assoc* 65:930–945.
- Mosimann JE, James FC. 1979. New statistical methods for allometry with application to Florida red-winged blackbirds. *Evolution* 33:444–459.
- Nelson JB. 1978. *The Sulidae: Gannets and Boobies*. Oxford: Oxford University Press.
- Nelson JB. 2005. *Pelicans, Cormorants, and their Relatives*. New York: Oxford University Press. 661 p.
- Niemi GJ. 1985. Patterns of morphological evolution in bird genera of new-world and old-world peatlands. *Ecology* (Washington DC) 66:1215–1228.
- Norberg UM. 1985. Flying, gliding, and soaring. In: Hildebrand M, Bramble DM, Liem KF, Wake DB, editors. *Functional Vertebrate Morphology*. Cambridge, MA: Harvard University Press. pp 129–158.
- O'Connor PM. 2009. Evolution of Archosaurian body plans: Skeletal adaptations of an air-sac based breathing apparatus in birds and other Archosaurs. *J Exp Zool* 311A:504–521.
- Owre OT. 1967. Adaptations for Locomotion and Feeding in the Anhinga and the Double-Crested Cormorant. American Ornithological Union, Ornithological Monograph, No. 6.
- Paradis E, Claude J, Strimmer K. 2004. APE: Analyses of phylogenetics and evolution in R language. *Bioinformatics* 20:289–290.
- Pennycuik CJ. 1972. Soaring behavior and performances of some East African Birds, observed from a motor-glider. *Ibis* 114:178–218.
- Pennycuik CJ. 1983. Thermal soaring compared in two dissimilar tropical bird species. *J Exp Biol* 102:307–325.
- Pennycuik CJ. 1990. Predicting wingbeat frequency and wavelength in birds. *J Exp Biol* 150:171–187.
- R Development Core Team (2009). *R: A language and environment for statistical computing*. Vienna: R Foundation for Statistical Computing. Available at <http://www.R-project.org>.
- Rayner JMV, 1988. Form and function in avian flight. In: Johnston RF, editor. *Current Ornithology*, Vol. 5. New York: Plenum Press. pp 1–66.
- Rayner JMV, Viscardi PW, Ward S, Speakman JR. 2001. Aerodynamics and energetics of intermittent flight in birds. *Am Zool* 41:188–204.
- Revell LJ. 2009. Size-correction and principal components for interpecific comparative studies. *Evolution* 63:3258–3268.
- Revell LJ, Harrison AS. 2008. PCCA: A program for phylogenetic canonical correlation analysis. *Bioinformatics* 24:1018–1020.
- Roark RJ, Young WC. 1975. *Formulas for Stress and Strain*, 5th ed. New York: McGraw Hill. 624 p.
- Rohlf FJ. 2001. Comparative methods for the analysis of continuous variables: Geometric interpretations. *Evolution* 55:2143–2160.
- Ropert-Coudert Y, Gremillet D, Ryan PG, Kato A, Naito Y, Le Maho Y. 2004. Between air and water: The plunge-dive of the cape gannet *Morus capensis*. *Ibis* 146:281–2901.
- Ruff CB, Hayes WC. 1983. Cross-sectional geometry of Pecos Pueblo femora and tibiae—A biomechanical investigation: I. method and general patterns of variation. *Am J Phys Anthropol* 60:359–381.
- Ruff CB. 2002. Long bone articular and diaphyseal structure in old world monkeys and apes. I: locomotor effects. *Am J Phys Anthropol* 119:305–342.
- Ryan PG. 2007. Diving in shallow water: The foraging ecology of darters (Aves: Anhingidae). *J Avian Biol* 38:507–514.
- Schnell GD. 1974. Flight speeds and wingbeat frequencies of the magnificent frigatebird. *Auk* 91:564–570.
- Schreiber RW, Woolfenden GE, Curtsinger WE. 1975. Prey capture by the Brown pelican. *Auk* 92:649–654.
- Siegel-Causey D. 1988. Phylogeny of the Phalacrocoracidae. *Condor* 90:885–905.
- Simons ELR. 2010. Forelimb skeletal morphology and flight mode evolution in pelecaniform birds. *Zoology* 113:39–46.
- Swartz SM, Bennett MB, Carrier DR. 1992. Wing bone stresses in free flying bats and the evolution of skeletal design for flight. *Nature* 359:726–729.
- Taylor MA. 1994. Stone, bone or blubber? Buoyancy control strategies in aquatic tetrapods. In: Maddock L, Bone Q, Rayner JMV, editors. *Mechanics and Physiology of Animals Swimming*. Cambridge: Cambridge University Press. pp 151–161.
- Wiemerskirch H, Le Corre, M, Bost CA. 2008. Foraging strategy of masked boobies from the largest colony in the world: Relationship to environmental conditions and fisheries. *MEPS* 362:291–302.